ISSN 1674-1056
http://cpb.iphy.ac.cn
http://iopscience.iop.org/cpb
中国物理 B
Chinese Physics
中国物理
Chinese Physics B

Novel infrared differential optical absorption spectroscopy remote sensing system to measure carbon dioxide emission

Ru-wen Wang(王汝雯), Pin-hua Xie(谢品华), Jin Xu(徐晋), Ang Li(李昂)

Citation: Chin. Phys. B . 2019, 28(1): 013301. **doi:** 10.1088/1674-1056/28/1/013301
Journal homepage: http://cpb.iphy.ac.cn; http://iopscience.iop.org/cpb

What follows is a list of articles you may be interested in

Room-temperature continuous-wave interband cascade laser emitting at 3.45 μm

Yi Zhang(张一), Fu-Hui Shao(邵福会), Cheng-Ao Yang(杨成奥), Sheng-Wen Xie(谢圣文), Shu-Shan Huang(黄书山), Ye Yuan(袁野), Jin-Ming Shang(尚金铭), Yu Zhang(张宇), Ying-Qiang Xu(徐应强), Hai-Qiao Ni(倪海桥), Zhi-Chuan Niu(牛智川)

Chin. Phys. B . 2018, 27(12): 124207. **doi:** 10.1088/1674-1056/27/12/124207

Generation of few-cycle radially-polarized infrared pulses in a gas-filled hollow-core fiber

Rui-Rui Zhao(赵睿睿), Zhi-Yuan Huang(黄志远), Ding Wang(王丁), Yu Zhao(赵钰), Yu-Xin Leng(冷雨欣), Ru-Xin Li(李儒新)

Chin. Phys. B . 2018, 27(10): 104204. **doi:** 10.1088/1674-1056/27/10/104204

Double-rod metasurface for mid-infrared polarization conversion

Yang Pu(蒲洋), Yi Luo(罗意), Lu Liu(刘路), De He(何德), Hongyan Xu(徐洪艳), Hongwei Jing(景洪伟), Yadong Jiang(蒋亚东), Zhijun Liu(刘志军)

Chin. Phys. B . 2018, 27(2): 024202. **doi:** 10.1088/1674-1056/27/2/024202

Self-compression of 1.8-μm pulses in gas-filled hollow-core fibers

Rui-Rui Zhao(赵睿睿), Ding Wang(王丁), Yu Zhao(赵钰), Yu-Xin Leng(冷雨欣), Ru-Xin Li(李儒新)

Chin. Phys. B . 2017, 26(10): 104206. **doi:** 10.1088/1674-1056/26/10/104206

Kerr-lens mode-locked polycrystalline Cr: ZnS femtosecond laser pumped by a monolithic Er: YAG laser

Chengfeng Hu(胡呈峰), Jiangfeng Zhu(朱江峰), Zhaohua Wang(王兆华), Xintong Sun(孙芯彤), Long Wei(魏龙), Weijun Ling(令维军), Zhong Dong(董忠), Qing Wang(王庆), Chunqing Gao(高春清), Zhiyi Wei(魏志义)

Chin. Phys. B . 2017, 26(1): 014206. **doi:** 10.1088/1674-1056/26/1/014206

Novel infrared differential optical absorption spectroscopy remote sensing system to measure carbon dioxide emission*

Ru-Wen Wang(王汝雯)[1,2], Pin-Hua Xie(谢品华)[1,2,3,†], Jin Xu(徐晋)[1,‡], and Ang Li(李昂)[1]

[1] *Key Laboratory of Environmental Optics and Technology, Anhui Institute of Optics and Fine Mechanics, Chinese Academy of Sciences, Hefei* 230031, *China*

[2] *University of Science and Technology of China, Hefei* 230026, *China*

[3] *CAS Center for Excellence in Urban Atmospheric Environment, Institute of Urban Environment, Chinese Academy of Sciences, Xiamen* 361021, *China*

(Received 18 September 2018; revised manuscript received 18 October 2018; published online 21 December 2018)

A CO_2 infrared remote sensing system based on the algorithm of weighting function modified differential optical absorption spectroscopy (WFM-DOAS) is developed for measuring CO_2 emissions from pollution sources. The system is composed of a spectrometer with band from 900 nm to 1700 nm, a telescope with a field of view of 1.12°, a silica optical fiber, an automatic position adjuster, and the data acquisition and processing module. The performance is discussed, including the electronic noise of the charge-coupled device (CCD), the spectral shift, and detection limits. The resolution of the spectrometer is 0.4 nm, the detection limit is 8.5×10^{20} molecules·cm^{-2}, and the relative retrieval error is $< 1.5\%$. On May 26, 2018, a field experiment was performed to measure CO_2 emissions from the Feng-tai power plant, and a two-dimensional distribution of CO_2 from the plume was obtained. The retrieved differential slant column densities (dSCDs) of CO_2 are around 2×10^{21} molecules·cm^{-2} in the unpolluted areas, 5.5×10^{21} molecules·cm^{-2} in the plume locations most strongly affected by local CO_2 emissions, and the fitting error is less than 2×10^{20} molecules·cm^{-2}, which proves that the infrared remote sensing system has the characteristics of fast response and high precision, suitable for measuring CO_2 emission from the sources.

Keywords: weighting function modified differential optical absorption spectroscopy (WFM-DOAS), infrared, instrument, CO_2 emission sources

PACS: 33.20.Ea, 07.88.+y, 42.87.–d, 42.72.Ai **DOI:** 10.1088/1674-1056/28/1/013301

1. Introduction

The carbon cycle is one of the most important material circulation systems on Earth. Its response to the growth of CO_2 and global warming is an important basis for future climate change prediction. In the natural cycle, carbon is transported between the atmosphere, the oceans and the terrestrial biosphere at a rate of about 10 billion tons per year.[1] Anthropogenic carbon increase has made a relatively small contribution in the past 200 years when compared to the considerable amount of carbon produced due to the combustion of fossil fuels, deforestation and the industrial production of cement, lime, ammonia, etc., all of which affect the natural cycle. During this time, the CO_2 concentration in the atmosphere has risen by about 30%, from 270 ppmv to 370 ppmv first, and now to 400 ppmv. Only about half of the anthropogenic carbon released into the atmosphere remains there, while the rest is absorbed by the marine and terrestrial biospheres.[2,3] The carbon has reached deep into the sea, and has been thought of as being removed from the environment (over a period of time of nearly one hundred years), but the carbon isolated by the biosphere could then be released back into the atmosphere in a shorter period of time. Therefore, changes and efficiencies in the fluxes about the oceans and terrestrial areas will be crucial for determining future CO_2 concentrations. However, CO_2 is a well-mixed and long-lived chemically inert gas in the atmosphere, whose distribution is affected by the transport process, including both natural and anthropogenic influences. Therefore, accurate measurement of CO_2 has become a challenge.[4–6]

Over the past few years, the CO_2 global monitoring data have been obtained mainly from satellites (such as the greenhouse gas observing satellite (GOSAT), the scanning imaging absorption spectrometer for atmospheric chartography (SCIAMACHY), the Chinese carbon dioxide observation satellite (TanSat), orbiting carbon observatory 2 (OCO-2), etc.), from the terrestrial total carbon column observing network (TCCON), and from some airborne flight tests.[7–13] Satellites have a wide range (i.e., 60 km × 30 km for SCIAMACHY, 10 km diameter for GOSAT and the thermal and near infrared sensor for carbon observation Fourier-transform spectrometer (Tanso-FTS), and 3.4 km^2 for OCO-2), but low precision, and single local emissions cannot be accurately resolved in the currently available satellite observational systems. In order to improve the retrieval accuracy, a variety of sensitivity analyses

*Project supported by the Key Program of the National Natural Science Foundation of China (Grant No. 41530644).

†Corresponding author. E-mail: phxie@aiofm.ac.cn

‡Corresponding author. E-mail: jxu@aiofm.ac.cn

© 2019 Chinese Physical Society and IOP Publishing Ltd

have been conducted to assess whether satellite instruments can achieve 1% accuracy, and these are mainly focused on obtaining total columns from the infrared (IR) using differential optical absorption spectroscopy (DOAS)[14–18] or from CO_2 thermal infrared emission bands.[19] The thermal infrared light comes from the middle troposphere, which is different from the IR radiation of sunlight. Therefore, the near-surface sensitivity of the IR radiation makes it an ideal spectral region to observe surface fluxes (although the 4 μm and 15 μm absorption bands are stronger);[20] moreover, IR is less sensitive to temperature and moisture. The TCCON has the advantage of high precision and the disadvantages of small coverage area, high cost and immobility, and it cannot provide information of source emissions. The retrieval band of TCCON is also the IR band. Therefore, neither the existing ground-based nor satellite observation systems can sufficiently contribute resolutions to small "hot-spot" areas and single facilities.

From the deficiencies in our current knowledge of point sources and "hot-spot" areas emerges a clear need for the development of a new measurement technique to improve estimates and constrain regional and local emissions. In this study, we have designed a CO_2 IR remote sensing system using a grating spectrometer (grating constant 600/mm). The spectrometer is thermoelectric cooling (the minimum temperature is −70 °C). The measurement band is 900–1700 nm, including two CO_2 absorption bands, with a central band of 1570 nm and 1600 nm, respectively. The resolution is about 0.35–0.5 nm and the slit width is adjustable between 10 μm and 100 μm. Solar light is the light source which is collected by a telescope with a field of view of 1.12°. Before entering the spectrometer, solar light goes through an optical fiber of about 5 m. The temperature, integration time, signal to noise ratio and detection limit of the instrument system are tested and analyzed in detail. In combination with the weighting function modified differential optical absorption spectroscopy (WFM-DOAS) algorithm, the spectra collected in the Feng-tai power plant are retrieved and the CO_2 slant column density is obtained as 2.0–5.5 molecules·cm^{-2}, the retrieval residue is 0.2%–0.6%, and the retrieval accuracy is 2%–4%. At the same time, we have obtained the plume spread distribution, which proves that the IR remote sensing system has the characteristics of fast response, easy operation, mobility and high precision.

2. Measurement principle and instrument

2.1. WFM-DOAS principle

Weighting function modified differential optical absorption spectroscopy is mainly employed to retrieve the total concentration of CO, CH_4, CO_2, H_2O and N_2O in the near-infrared (NIR) for SCIAMACHY.[14–16] Subsequently, WFM-DOAS was succeeded by global ozone monitoring experiment (GOME) data inversion to obtain the total ozone column.[21] At the same time, the water vapor column density near 700 nm was obtained from SCIAMACHY satellite and GOME satellite spectral retrieval.[22] The basic principle of WFM-DOAS is least squares fitting, as shown in the equation given below this paragraph, where the summation of the logarithm of the reference spectrum and the first derivative of the interfering component are taken, a second-order polynomial is subtracted from the logarithm of the value of the measured spectrum, and least squares fitting on this difference is performed to obtain the best solution. In the equation given below, subscript i refers to each detector pixel of the central wavelength λ_i, I_i^{meas} and I_i^{ref} refer to the normalized measurement spectrum and reference spectrum, respectively, $V^{\text{t}} = \left(V^{\text{t}}_{\text{CO}_2}, V^{\text{t}}_{\text{H}_2\text{O}}, V^{\text{t}}_{\text{Temp}}\right)$ represents the true vertical column, $\bar{V} = (\bar{V}_{\text{CO}_2}, \bar{V}_{\text{H}_2\text{O}}, \bar{V}_{\text{Temp}})$ represents the vertical column model simulation, $\hat{V}_j$ represents the retrieved vertical columns (the subscript j stands for CO_2, H_2O, or temperature (Temp)), and $P_i(a_{\text{m}})$ represents the effect of broadband structures, such as aerosol and ground reflectance, on the retrieval results. In this study, the 1590–1620 nm band is selected as the retrieval band. The main interference factors are H_2O, Temp, and CH_4.

$$\left\| \ln I_i^{\text{meas}}\left(V^{\text{t}}\right) - \left[\ln I_i^{\text{ref}}\left(\bar{V}\right) + \frac{\partial \ln I_i^{\text{ref}}}{\partial \bar{V}_{\text{CO}_2}}\left(\bar{V}_{\text{CO}_2} - \hat{V}_{\text{CO}_2}\right) + \frac{\partial \ln I_i^{\text{ref}}}{\partial \bar{V}_{\text{H}_2\text{O}}}\left(\bar{V}_{\text{H}_2\text{O}} - \hat{V}_{\text{H}_2\text{O}}\right) + \frac{\partial \ln I_i^{\text{ref}}}{\partial \bar{V}_{\text{Temp}}}\left(\bar{V}_{\text{Temp}} - \hat{V}_{\text{Temp}}\right) + P_i(a_{\text{m}}) \right] \right\|^2 \equiv \|\text{RES}_i\|^2 \rightarrow \min \text{ w.r.t } \hat{V}_j \ \& \ a_{\text{m}}.$$

2.2. Remote sensing system

A schematic diagram of the CO_2 IR remote sensing system is shown in Fig. 1. It contains two parts: one part is the spectral acquisition system, including IR spectrometer, InGaAs detector, telescope (both tube and inner wall are black in order to avoid transmitted and reflected light), 5-m-long optical fiber, and automatic position adjuster, and the other part is the data collection and processing system, i.e., the laptop. The IR spectrometer (Andor SR303i) is a high-performance grating spectrometer for weak light absorption. It can choose different coupling methods or combine with different types of detectors according to different needs. It adopts triple raster wheel design, and is not required to change other raster and redo optical calibration. In addition, the experimental operation is simple. The detector is an Andor iDus depth-cooled InGaAs 1024 array detector with a compact design, dedicated vacuum seal and dedicated deep thermoelectric (TE) cooling, which can acquire a minimum temperature of −70 °C. It is stable and easy to use, with a photon efficiency of 80% ± 5%

in the 900–1650 nm band. The basic parameters of the system are tabulated in Table 1.

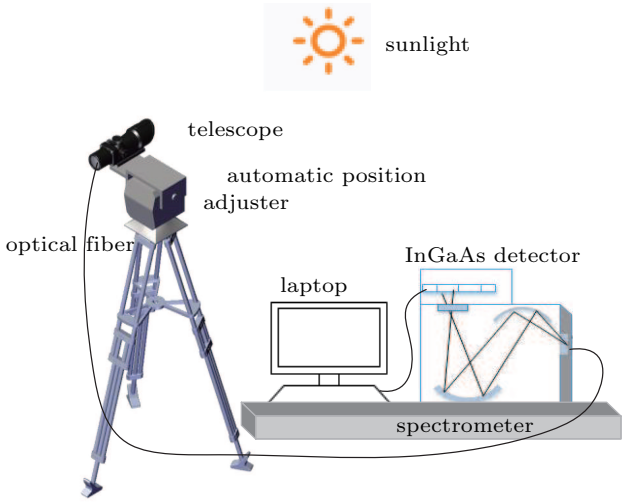


Fig. 1. Schematic diagram of the CO_2 IR remote sensing system.

Table 1. The parameters of the CO_2 NIR remote sensing system.

Measurement band/nm	900–1700
Spectral range/nm	1590–1620
Focal length f/mm	303
Aperture/mm	f/4
Grating	600/mm
Spectral resolution/nm	0.4
Photon efficiency/%	80% ± 5%
Instantaneous field of view (IFOV)/(°)	1.12
Filter band range/nm	1500–1700
Filter transmittance	90%
Detector	liquid nitrogen (LN) cooled (−90 °C) 1024 pixel InGaAs CCD

2.3. Remote sensing system performance test

Fitting residue is an important manifestation of the retrieval quality. As is known, residuals are mainly determined by measurement noise and system noise. The measurement noise originates from spectral calibration, spectral structure of the light source, the instrument measurement limitation, and so on. The system noise comes from the spectrometer and the type of connection between the telescope and spectrometer. In order to reduce the fitting residuals and improve retrieval accuracy, the basic performance testing of the spectrometer and IR remote sensing system is carried out at the beginning, including the measurement of the relationship between the temperature, dark current, and offset and integration time of the spectrometer; the whole system spectral calibration is performed and sample gas measurement is undertaken in the laboratory.

2.3.1. Spectrometer performance

The relationship between spectrometer temperature, dark current, and offset and integration time are depicted in Fig. 2. The spectrometer cools down slowly from 0 °C to −60 °C, and the dark current drops rapidly at −10 °C followed by a gradual drop until it is stabilized at 160 counts when the charge-coupled device (CCD) maintains a temperature below −50 °C. The temperature is maintained at −50 °C, while the integration time increases continuously from 0 to 2000 ms. With the increase of the integration time, the dark current exhibits a linear relationship with the integration time, i.e., $y = 0.17798x + 16.17$ ($R^2 = 0.99978$). Taking the minimum integration time of the spectrometer (1.4 μs) as the unit, the number of integrals increases continuously. The result shows that the average offset of different integral times is independent of the number of integrals and is a constant value of about 1260 counts/scan. In order to ensure the minimum noise signal during the acquisition of the spectra, firstly, the CCD temperature is stabilized at −50 °C to −70 °C; secondly, a certain integration time is achieved for a light intensity of at least 20000 counts; and thirdly, the signal to noise ratio is kept as high as possible while collecting the spectra, thereby reducing the system noise error.

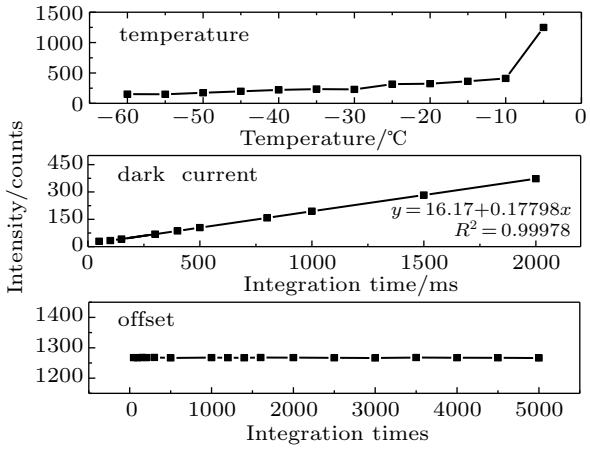


Fig. 2. Basic performance of the spectrometer: the relationship between temperature, dark current, and offset and integral time/integral number.

2.3.2. System spectral calibration

The 1590–1620 nm band is selected as the measurement band, and there are 1024 pixels corresponding to 104.07 nm. Taking 1600 nm as the center, the measurable waveband is 1547.87–1651.94 nm. The Kr lamp is used as the linear-infrared light source for calibration (the Kr lamp spectrum is shown in Fig. 3(a)). The Kr lamp is fixed on the bracket of the optical rail (the optical rail is perpendicular to the telescope) and moved to the position of the strongest signal and the best peak shape; the integration time is adjusted until the Kr lamp peak intensity is the strongest with the premise of being unsaturated, and the signal is acquired. Five peaks, namely 1568.1, 1582.009, 1589.0068, 1592.578 and 1631.5258, are selected as the reference values to calibrate, and the relationship between the pixel and wavelength $y = 1547.871 + 0.10166x$ ($R^2 = 0.9994$) is obtained, as shown in Fig. 3(b).

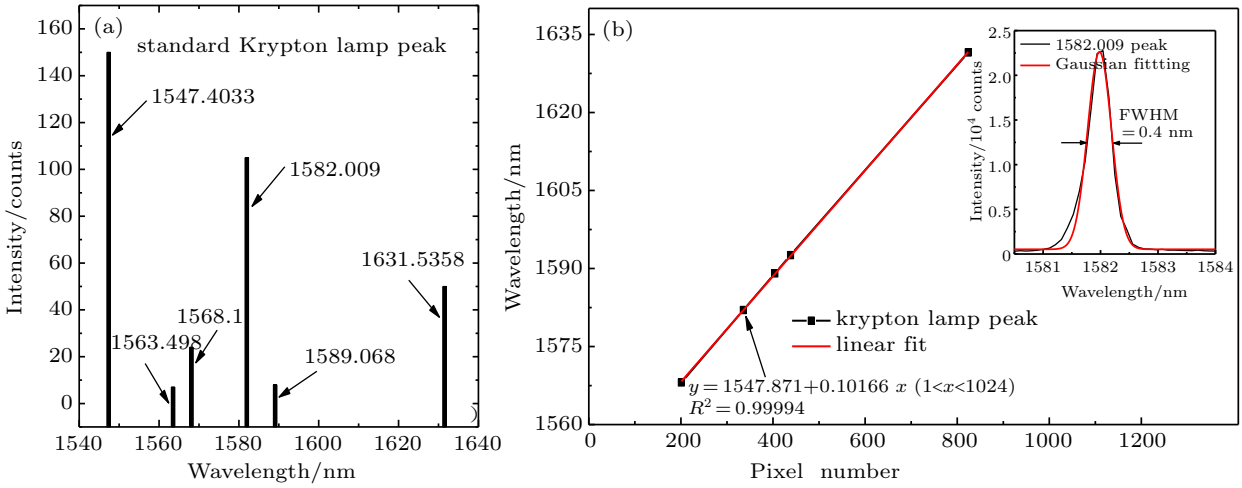


Fig. 3. (a) Standard Kr spectrum. (b) System calibration.

2.3.3. Sample gas measurement in the laboratory

In order to measure reference light spectra, the device is set up as shown in Fig. 4. A Xenon (Xe) lamp, which is a continuous light source in the 1550–1650 nm waveband with the advantages of large power and cost-effectiveness, is used as the light source. The sample cell is 100 cm long with a diameter of 3 cm, and the measurement temperature is 25 °C. First, N_2 is pumped into the sample cell to remove the air, and the process lasts for about 5 minutes. Then the N_2 intake rate is decreased down to 0.1 L/min. After one minute, 10 spectra of N_2 are collected as the reference spectra. Samples of CO_2 with the measurements 0.1, 0.2, 0.3, 0.5, 0.6, 0.7 and 1.0 million ppmv are poured into the cell to obtain a series of sample gas spectra. All measurement absorption spectra are divided by the reference spectra, and the data are converted into optical density values by taking the logarithm of the quotients thus obtained. The sample gas spectrum retrievals are performed using CO_2 absorption cross-sections at 25 °C acquired from a database to obtain the CO_2 column density. Since for the lamp spectra it is assumed that there is no CO_2 absorption, the fitting coefficients obtained from spectral retrieval are gas column densities. By dividing the gas column densities by the optical path, a mixing ratio is obtained, which is calculated based on the actual pressure and temperature of the sample gas. By comparing with the standard sample gas values, the retrieval error and retrieval accuracy are obtained, and the details are shown in Table 2. The sample gas spectrum of 7×10^5 ppmv fitting result is taken as an example, which is shown in Fig. 5.

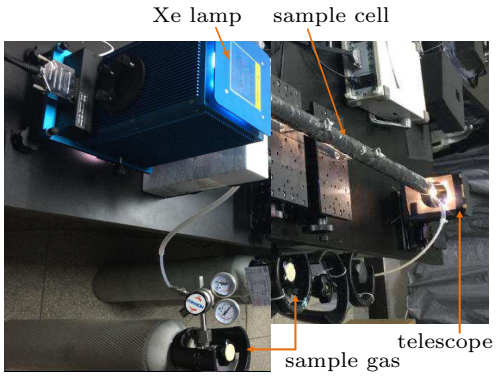


Fig. 4. Sample gas measurement device in the laboratory.

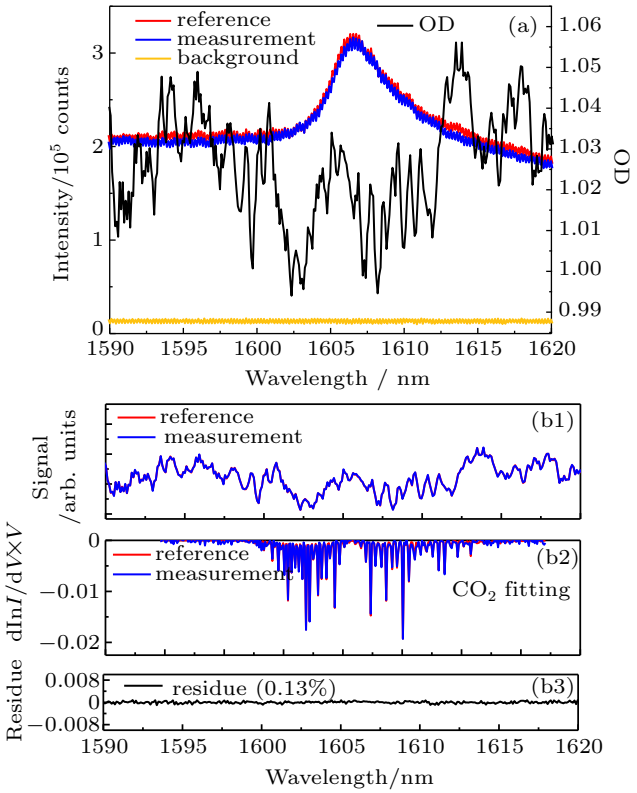


Fig. 5. Example of 7×10^5 ppmv. (a) The sample gas measurement spectrum along with reference and background spectra, where OD indicates optical density; (b) retrieval results.

In Fig. 5, red and black lines represent the reference and measured values, respectively. Through retrieval, we obtain the sample gas column concentration, which is $1.827 \times 10^{21} \pm 8.98 \times 10^{19}$ molecules·cm^{-2}, when the theoretical value is 1.876×10^{21} molecules·cm^{-2}; the retrieval residue is 0.13%,

and retrieval accuracy is 3.6%. As shown in Fig. 6, when the CO_2 concentration is less than 7×10^5 ppmv, the theoretical value is close to the measured value. With the increase of the sample gas concentration, the measured CO_2 column density no longer increases linearly. When the CO_2 concentration is less than 3×10^5 ppmv, the detector cannot measure the spectral absorption, that is, the detection limit of the system is 8.5×10^{20} molecules·cm^{-2}. Converting the limited column density into the atmosphere CO_2 column without emission sources, we can conclude that the effective optical length of the spectral absorption is at least 1 km when we assume that X_{CO_2} (volume mixing ratio of CO_2) is 400 ppmv in the atmosphere.

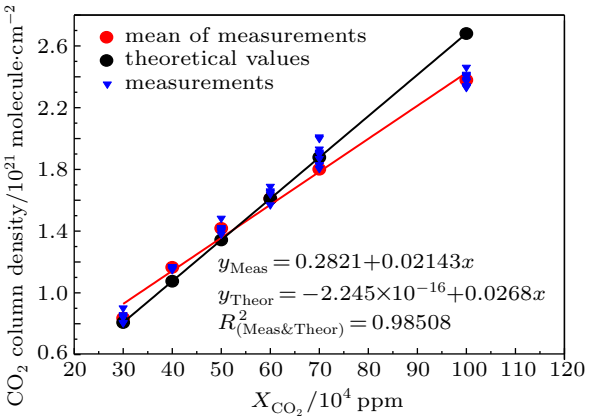


Fig. 6. Linear relationship between the measured and theoretical values of different concentrations of sample gas.

Table 2. CO_2 measurement and relative errors.

CO_2 density/million ppm	Number of measurements	1	2	3	4	5	Average/million ppm
0.1	measurement	0.1046	0.1018	0.097	0.097	0.099	0.099
	relative error/%	4.6	1.82	3	3	1	1
0.2	measurement	0.198	0.199	0.197	0.206	0.204	0.2008
	relative error/%	1	0.5	1.5	3	2	0.4
0.3	measurement	0.294	0.289	0.299	0.298	0.298	0.2956
	relative error/%	2	3.7	0.4	0.7	0.7	1.5
0.5	measurement	0.498	0.499	0.475	0.501	0.502	0.495
	relative error/%	0.4	0.1	5	0.2	0.4	1
0.6	measurement	0.599	0.598	0.602	0.61	0.596	0.501
	relative error/%	0.2	0.4	0.3	1.6	0.7	1.6
0.7	measurement	0.698	0.701	0.72	0.709	0.698	0.705
	relative error/%	0.3	0.1	2.8	1.28	0.3	0.7
1.0	measurement	0.988	0.987	0.98	0.982	0.97	0.98
	relative error/%	1.2	1.3	2	1.8	3	2

3. Field campaign and data analysis

3.1. Field of view

A sketch of the experimental site and the viewing method is shown in Fig. 7. Observations were carried out at a distance of about 1000 m and 1200 m away from the power plant chimneys at 11:00 am on May 26, 2018, measuring the solar radiation that is backscattered by the plume or atmosphere to the entrance objective. There was no other pollution source nearby. Two chimneys, 140 m high, with respective widths of 12 m and 18 m, were spaced about 138 m apart. The weather was clear with a wind speed of about 1.5 m/s.



Fig. 7. Experimental site at the Feng-tai power plant.

3.2. Data analysis

The power plant emission measurements presented in this study were carried out with the IR differential optical absorption spectroscopy remote sensing system instrument (refer to Section 2), which measures in multiple azimuthal and elevation viewing directions, pointing directly towards the plume while different viewing azimuth angles and elevation angles cover a large part of the region. We select the zenith light as the reference spectra. The data retrieval results are shown in Fig. 8 and the retrieval error in Fig. 9. During the measurement, the retrieved differential slant column densities (dSCDs) of CO_2 are around 2×10^{21} molecules·cm^{-2} for the areas which are similarly unpolluted as the rural reference region, and 5.5×10^{21} molecules·cm^{-2} for locations most strongly affected by local CO_2 emissions. In addition, most of the retrieval errors are lower than 2×10^{20} molecules·cm^{-2}; retrieval precision is better than 4%. All spectra in this section are obtained in 0.7 s exposure time.

The locations of the two maximum values are marked in Fig. 8 by two black dots. Our observation site is about 1000 meters away from the chimney; hence, we can calculate the

height of the two maximum values which is about 140.5 m, matching the chimney height of 140 m. During the observation, our instrument was located at a point with an azimuthal angle of 40°. Through geometric calculation, we calculate that the distance between the two chimneys is about 131.8 meters, which agrees well with the chimney distance of 138 m. It is obvious that the first maximum is in good agreement with the mouth of the chimney. There are two reasons for this: one is that the observation angle is exactly at the top of the chimney; and the other is that the chimney has not been improved for efficiency. Therefore, the first chimney emits more CO_2, which can explain the two high values marked by a red dot on the right of the first chimney. Another maximum value appears on the left of the second chimney owing to the plume accumulated there. One part of the plume is blown by the wind from the first chimney, and the other part comes from the plume spread of the second chimney.

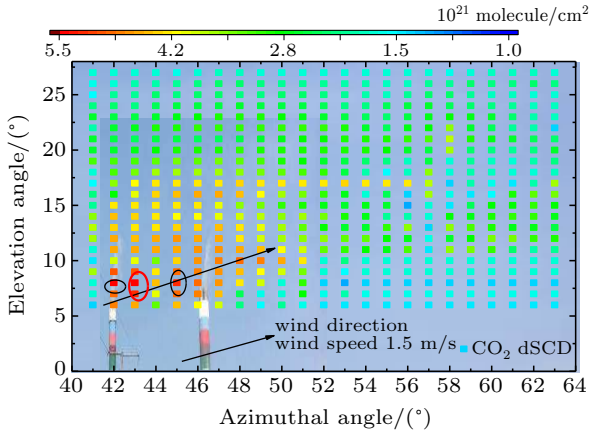


Fig. 8. CO_2 dSCD at different elevation and azimuthal angles.

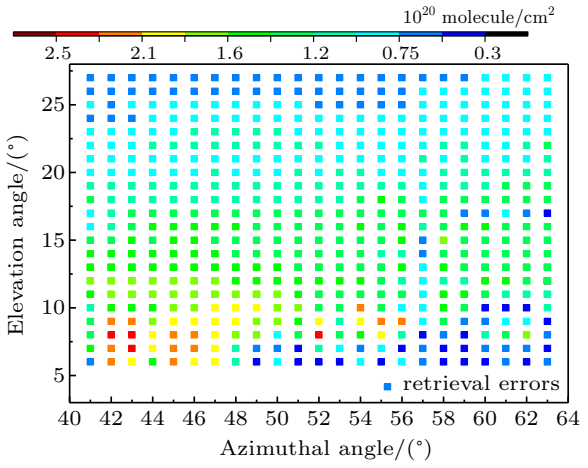


Fig. 9. CO_2 dSCD retrieval errors at different elevation and azimuthal angles.

Referring to the measurements in different azimuthal and vertical viewing directions, the movement direction of the plume can be easily distinguished, as shown in Fig. 8. During the observation, the wind speed is about 1.5 m/s stably at the height of 140 m, and the direction is east to north 45°, as shown in Fig. 8, so $v_{\parallel} = v_{\perp} = 1.06$ m/s. In the azimuthal direction, the plume spreads from 46.5° to 52°, which represents about 107.45 m. We can calculate the spread time, which is about 100 s, because $v_{\parallel}$ can be supposed to be fixed. In the vertical direction, the plume spreads from 7° to 18°, which represents about 202.12 m. The plume is approximately 100 meters high from the chimney, because the plume speed from the chimney is nearly 10 m/s; though the speed decreases as the height increases, the spread distance is still longer than the azimuthal direction.

4. Conclusion

The CO_2 IR remote sensing system is a passive remote sensing instrument to measure CO_2 column amounts from emission sources, with a precision of $\leqslant 4\%$. The resolution of the system is 0.4 nm, the detection limit is 8.5×10^{20} molecules·cm^{-2}, and the relative retrieval error is $< 1.5\%$ for a cylindrical sample cell size 100 cm $\times\, 3^2\pi$ cm^2 and a sample gases density of less than 10^6 ppmv. Through the field experiment, we obtain the retrieval results and the plume spread distribution, showing that the IR remote sensing system has the ability to quantify point source emissions from power plants in a short time with high precision. Other CO_2 point sources, such as steel factories, can also be quantified with this instrument. The application of this system can deliver important information about greenhouse gas emission sources for carbon emission statistics and climate prediction.

References

[1] Houghton J T, Ding Y, Griggs D J, Noguer M, van der Linden P J, Dai X, Maskell K and Johnson C A 2001 *IPCC: Climate Change 2001: The Scientific Basis* (Cambridge: Cambridge University Press) p. 881
[2] Sabine C L, Freely R A, Gruber N, Key R M, Lee K, Bullister J L, Wanninkhof R, Wong C S, Wallace D W R, Tilbrook B, Millero F J, Peng T H, Kozyr A, Ono T and Roso A F 2004 *Science* **305** 367
[3] Saunois M, Jackson, R B Bousquet P, Poulter B and Canadell J G 2016 *Environ. Res. Lett.* **11** 120207
[4] Krings T, Gerilowski K, Buchwitz M, Reuter M, Tretner A, Erzinger J, Heinze D, Pfluger U, Burrows J P and Bovensmann H 2011 *Atmos. Meas. Tech.* **4** 1735
[5] Zhang F, Zhou L X and Xu L 2013 *Sci. Chin. Earth Sci.* **56** 727
[6] García M Á, Sánchez M L, Pérez I A, Ozores M I and Pardo N 2016 *Sci. Total Environ.* **550** 157
[7] Gottwald M and Bovensmann H 2011 *SCIAMACHY - Exploring the Changing Earth's Atmosphere* (Netherlands: Springer) pp. 176–216
[8] Frankenberg C, Pollock R, Lee R A M, Rosenberg R, Blavier J F, Crisp D, O'Dell C W, Osterman G B, Roehl C, Wennberg P O and Wunch D 2015 *Atmos. Meas. Tech.* **8** 301
[9] Houweling S, Hartmann W, Aben I, Schrijver H, Skidmore J, Roelofs G J and Breon F M 2005 *Atmos. Chem. Phys.* **5** 3003
[10] Frankenberg C, Pollock R, Lee R A M, Rosenberg R, Blavier J F, Crisp D, O'Dell C W, Osterman G B, Roehl C, Wennberg P O and Wunch D 2015 *Atmos. Meas. Tech.* **8** 301
[11] Machida T 2008 *J. Atmos. Oceanic Technol.* **25** 1744
[12] Du J, Sun Y G, Chen D J, Mu Y J, Huang M J, Yang Z G, Liu J Q, Bi D C, Hou X and Chen W B 2017 *Chin. Opt. Lett.* **15** 031401
[13] Wang Z, Chen S, Yang C and Wang M 2011 *Chin. Opt. Lett.* **9** 020101

[14] Buchwitz M, de Beek R, Bramstedt K, Noël S, Bovensmann H and Burrows J P 2004 *Atmos. Chem. Phys.* **4** 1945
[15] Buchwitz M, de Beek R, Burrows J P, Bovensmann H, Warneke T, Notholt J, Meirink J F, Goede A P H, Bergamaschi P, Körner S, Heimann M and Schulz A 2005 *Atmos. Chem. Phys.* **5** 941
[16] Buchwitz M, de Beek R, Noël S, Burrows J P, Bovensmann H, Bremer H, Bergamaschi P, Körner S and Heimann M 2005 *Atmos. Chem. Phys.* **5** 3313
[17] Gong W, Liang A L, Han G, Ma X and Xiang C Z 2015 *Photon. Res.* **3** 146
[18] Gong W, Xiang C Z, Mao F Y, Ma X and Liang A L 2016 *Photon. Res.* **4** 74
[19] Chédin A, Saunders R, Hollingsworth A, Scott N A, Matricardi M, Etcheto J, Clerbaux C, Armante R and Crevoisier C 2003 *J. Geophys. Res.* **108** 4064
[20] Barkley M P, Frieß U and Monks P S 2006 *Atmos. Chem. Phys.* **6** 3517
[21] Coldewey-Egbers M, Weber M, Buchwitz M and Burrows 2004 *Adv. Space Res.* **34** 749
[22] Noël S, Buchwitz M and Burrows J P 2004 *Atmos. Chem. Phys.* **4** 111